Unsteady MHD Chemically Reactive Flow of a Methanol blended Casson Fluid over an Exponentially Stretching Surface

C. Arruna Nandhini [*1], S. Jothimani [2]

Department of Mathematics, Government Arts College (Autonomous), Coimbatore – 641 018

* Corresponding author: arruna98@gmail.com

Article Info
Page Number: 2248-2260
Publication Issue:
Vol. 71 No. 4 (2022)

Article History
Article Received: 25 March 2022
Revised: 30 April 2022
Accepted: 15 June 2022
Publication: 19 August 2022

Abstract
In the current study, a breakthrough approach of investigating the impact of chemical reaction and heat source/sink in an unsteady flow of Casson fluid with methanol, past an exponentially stretching surface was first proposed. Appurtenant similarity variables are adopted to transfigure the governing partial differential equations into a system of ordinary differential equations. Subsequently, numerical solutions to these equations are found. The repercussions of the physical components that affect the flow, heat and mass transmission phenomena are sketched, tabulated and scrutinized briefly.
Keywords: Unsteady Casson fluid; Exponentially stretching surface; Chemical reaction; Heat source/sink.

Introduction

First and foremost, Crane [1] discovered the exact solution of steady flow past a sheet that is being stretched. The majority of the extant literature focuses on linearly stretching sheet. Nevertheless, it is often alleged that, realistically, the rate of surface stretching might not essentially be linear in real-world scenarios. There may be circumstances where the sheet stretches in an exponential order. Several investigators [2 – 5] focused on the boundary layer heat transmission over an exponentially stretching sheet.

It is well known that Mathematicians, physicists and engineers lay great emphasis on the mechanics of non-Newtonian fluids. The simplest subclass among the non-Newtonian models is the Casson fluid, whose flow (such as blood and certain oils) possesses distinctive features and has gained recent prominence. Numerous authors investigated the Casson fluid's boundary layer flow in a variety of configurations. Mukhopadhyay et al. [6] and Mahdy [7] numerically elicited the unsteady Casson fluid across a stretching sheet under different conditions.

Methanol is envisioned as the future fuel. Recent advances show that blending methanol with vegetable oil is characterised as the most cost-effective and environment-friendly fuel. Despite the overwhelming importance, no attempt has been made to analyse the flow of unsteady chemically reactive methanol mixed with Casson fluid across an exponentially stretching surface accompanied by a uniform heat source or sink. The impact of several dimensionless pertinent parameters on the velocity profile, temperature and concentration distributions are analysed through tables and graphs.

Nomenclature

μ	Dynamic viscosity	ν	Kinematic viscosity
σ	Electrical conductivity	ρ	Density
κ	Thermal conductivity	q_r	Radiative heat flux
ρc_p	Heat capacitance	t	Time factor
Q^*	Heat source / sink	N	Exponential parameter
σ^*	Stefan-Boltzmann Constant	k^*	Mean absorption coefficient
T	Temperature	C	Concentration
T_0	Reference temperature	C_0	Reference concentration
T_∞	Ambient temperature	C_∞	Ambient concentration
g	Acceleration due to gravity	L	Characteristic length
$V(x)$	Suction/injection	ψ	Stream function
η	Similarity variable	θ	Dimensionless temperature
ϕ	Dimensionless concentration	C_f	skin friction coefficient
Nu_x	Local Nusselt number	Sh_x	Local Sherwood number
A	Unsteadiness parameter	M	Magnetic field parameter
Gr	Thermal Grashof number	Gc	Concentration Grashof number
R	Radiation parameter	Q	Heat source/sink parameter
Ec	Eckert number	Sc	Schmidt number
k	Chemical reaction parameter	s	Suction/injection parameter
β	Casson fluid parameter	D_m	Diffusion coefficient
Re_x	Local Reynolds number	Q_0	Initial value of heat source / sink
μ_B	plastic dynamic viscosity	P_y	yield stress
τ_{ij}	$(i,j)^{th}$ component of stress tensor	e_{ij}	Deformation rate's $(i,j)^{th}$ component
Pr	Prandtl number	k_l	rate of chemical reaction

Mathematical Formulation

Under consideration is a two-dimensional unsteady viscous flow of an electrically conducting, non-Newtonian Casson fluid past an exponentially stretching surface. As illustrated in Fig. 1, it is postulated that the exponentially stretching surface is positioned along the x-axis, and the y-axis is perpendicular to it. The fluid is subjected to a uniform transverse magnetic field $B(x,t) = \frac{B_0}{\sqrt{1-ct}} e^{\frac{Nx}{2L}}$, where B_0 is a constant. The exponential velocity is $U_w(x,t) = \frac{U_0}{1-ct} e^{\frac{Nx}{L}}$, the temperature at the surface is placed at $T_w(x,t) = T_\infty + \frac{T_0}{(1-ct)^2} e^{\frac{Nx}{2L}}$ and the surface concentration is $C_w(x,t) = C_\infty + \frac{C_0}{(1-ct)^2} e^{\frac{Nx}{2L}}$.

As propounded by Casson [8], the isotropic and incompressible Casson fluid flow's rheological equation of state is governed by the following equation:

$$\tau_{ij} = \begin{cases} 2\left(\mu_B + \frac{P_y}{\sqrt{2\pi}}\right)e_{ij} & \pi > \pi_c \\ 2\left(\mu_B + \frac{P_y}{\sqrt{2\pi_c}}\right)e_{ij} & \pi < \pi_c \end{cases} \quad (1)$$

From equation (1), $\pi = e_{ij}e_{ij}$ and in accordance with the non-Newtonian model, π_c is the critical value of π.

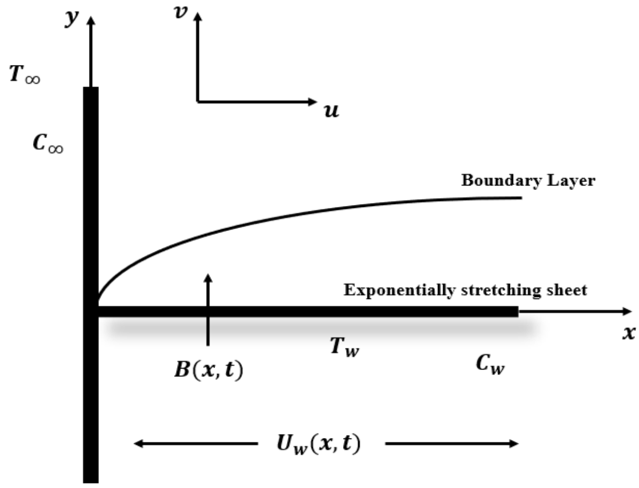

Fig. 1 Coordinate system of fluid flow

These suppositions lead to the standard Boussinesq approximation, which accrues the following governing equations for the prevailing flow.

$$\frac{\partial u}{\partial x} + \frac{\partial v}{\partial y} = 0 \quad (2)$$

$$\frac{\partial u}{\partial t} + u\frac{\partial u}{\partial x} + v\frac{\partial u}{\partial y} = \nu\left(1 + \frac{1}{\beta}\right)\frac{\partial^2 u}{\partial y^2} + g\beta_T(T - T_\infty) + g\beta_C(C - C_\infty) - \frac{\sigma B^2 u}{\rho} \quad (3)$$

$$\frac{\partial T}{\partial t} + u\frac{\partial T}{\partial x} + v\frac{\partial T}{\partial y} = \frac{1}{\rho c_P}\left[\kappa\frac{\partial^2 T}{\partial y^2} - \frac{\partial q_r}{\partial y} + \mu\left(1 + \frac{1}{\beta}\right)\left(\frac{\partial u}{\partial y}\right)^2 + Q^*(T - T_\infty) + \sigma B^2 u^2\right] \quad (4)$$

$$\frac{\partial C}{\partial t} + u\frac{\partial C}{\partial x} + v\frac{\partial C}{\partial y} = D_m\frac{\partial^2 C}{\partial y^2} - k_l(C - C_\infty) \quad (5)$$

In this instance, u and v are the x and y directional velocity components respectively. Also, $\beta = \frac{\mu_B\sqrt{2\pi_c}}{P_y}$, $Q^* = \frac{Q_0 e^{\frac{Nx}{L}}}{1-ct}$ and $k_l = \frac{k_0 e^{\frac{Nx}{L}}}{1-ct}$ where k_0 is a constant. Rosseland approximation [9] is employed to evaluate q_r which is as follows:

$$q_r = -\frac{4\sigma^*}{3k^*}\frac{\partial T^4}{\partial y}$$
(6)

It is presumed that the flow's internal temperature variations are suitably modest. Truncation of higher order terms after expanding T^4 using Taylor's series about T_∞ gives:

$$T^4 \equiv 4T_\infty^3 T - 3T_\infty^4$$
(7)

Equation (4) is modified by incorporating (6) and (7) to produce

$$\frac{\partial T}{\partial t} + u\frac{\partial T}{\partial x} + v\frac{\partial T}{\partial y} = \frac{\kappa}{\rho c_P}\frac{\partial^2 T}{\partial y^2} + \frac{16\sigma^* T_\infty^3}{3\rho c_P k^*}\frac{\partial^2 T}{\partial y^2} + \frac{\nu}{c_P}\left(1+\frac{1}{\beta}\right)\left(\frac{\partial u}{\partial y}\right)^2 + \frac{Q^*}{\rho c_P}(T - T_\infty) + \frac{\sigma B^2 u^2}{\rho c_P}$$
(8)

Boundary Conditions

The appurtenant boundary constraints can be expressed as

at $y = 0$: $u = U_w(x,t)$, $v = -V(x)$, $T = T_w(x,t)$, $C = C_w(x,t)$

as $y \to \infty$: $u \to 0$, $T \to T_\infty$, $C \to C_\infty$

At the wall, a peculiar kind of velocity $V(x)$ is taken into account [6]. Here $V(x) = V_0 e^{\frac{Nx}{2L}}$ where V_0 is a constant. In addition, $V(x) > 0$ and $V(x) < 0$ signifies the suction velocity and blowing (injection) velocity respectively. Also, the expressions for $U_w(x,t)$, $T_w(x,t)$ and $C_w(x,t)$ are valid only if $ct < 1$.

Method of Solution

The equation of continuity (2) is met by opting $\psi(x,y)$ such that $u = \frac{\partial \psi}{\partial y}$ and $v = -\frac{\partial \psi}{\partial x}$. The following similarity transformation is utilized to transmogrify the equations (3), (8) and (5).

$$\eta = \sqrt{\frac{U_0}{2\nu L(1-ct)}}\, e^{\frac{Nx}{2L}}\, y$$
(9a)

$$\psi(x,y) = \sqrt{\frac{2U_0\nu L}{1-ct}}\, e^{\frac{Nx}{2L}} f(\eta)$$
(9b)

$$\theta(\eta) = \frac{T - T_\infty}{T_w - T_\infty}$$
(9c)

$$\phi(\eta) = \frac{C - C_\infty}{C_w - C_\infty}$$
(9d)

The transformed set of ordinary differential equations take the following form:

$$\left(1+\frac{1}{\beta}\right)f''' - (A\eta - Nf)f'' - 2N{f'}^2 - 2(M+A)f' + 2Gr\theta + 2Gc\phi = 0 \tag{10}$$

$$\frac{1}{Pr}\left(1+\frac{4}{3}R\right)\theta'' - (A\eta - Nf)\theta' - (4A + Nf' + Q)\theta + Ec\left(1+\frac{1}{\beta}\right){f''}^2 + 2MEc{f'}^2 = 0 \tag{11}$$

$$\frac{1}{Sc}\phi'' - (A\eta - Nf)\phi' - (4A + Nf' + k)\phi = 0 \tag{12}$$

The associated boundary conditions after applying equation (9) are:

$$\text{at } \eta = 0 \ : \quad f(\eta) = s, \quad f'(\eta) = 1, \quad \theta(\eta) = 1, \quad \phi(\eta) = 1 \tag{13}$$

$$\text{as } \eta \to \infty : \quad f'(\eta) \to 0, \quad \theta(\eta) \to 0, \quad \phi(\eta) \to 0 \tag{14}$$

where the prime notation delineates the differentiation with respect to η.

The dimensionless parameters obtained during this transformation include:

$A = \frac{cL}{U_0 e^{\frac{Nx}{L}}}$, $M = \frac{\sigma B_0^2 L}{\rho U_0}$, $Gr = \frac{gL\beta_T(T_w - T_\infty)}{U_w^2}$, $Gc = \frac{gL\beta_C(C_w - C_\infty)}{U_w^2}$, $R = \frac{4\sigma^* T_\infty^3}{\kappa k^*}$, $Q = \frac{2LQ_0}{\rho c_p U_0}$, $Ec = \frac{U_w^2}{c_p(T_w - T_\infty)}$,

$Sc = \frac{\nu}{D_m}$, $k = \frac{2Lk_0}{U_0}$, $s = \frac{V(x)}{N\sqrt{\frac{\nu U_0}{2L(1-ct)}}\, e^{\frac{Nx}{2L}}}$ and $Pr = \frac{\nu}{\kappa}$.

The physical quantities of interest viz., C_f, Nu_x and Sh_x in the dimensionless form can be expressed as

$$\frac{C_f\sqrt{Re_x/2}}{\sqrt{x/L}} = \left(1+\frac{1}{\beta}\right)f''(0) \tag{15}$$

$$\frac{Nu_x}{\sqrt{Re_x/2}\sqrt{x/L}} = -\theta'(0) \tag{16}$$

$$\frac{Sh_x}{\sqrt{Re_x/2}\sqrt{x/L}} = -\phi'(0) \tag{17}$$

where $Re_x = \frac{xU_w}{\nu}$.

Results and Discussions

Numerical solutions are provided for the resulting transformed equations (10) – (12) and the boundary conditions (13) and (14) using MATLAB bvp4c inbuilt package. For the sake of brevity, the solutions of this present model have been illustrated through graphs and tables. The procured $f''(0)$ for ample values of A are reported in Table 1 so as to authenticate the precision of the numerical technique employed in this study. Table 2 was drawn under limiting conditions to compare the numerical values of $-\theta'(0)$ for several values of Pr and M when $N = 1$ and in the absence of other involved parameters. It is affirmed that the numerical findings of the current assessment were in very good accord with the existing literature. For numerical results, the fixed values of the pertinent parameters are taken as $A = 0.5,\ s = 0.1,\ \beta = 2,\ Ec = 0.01,\ Gr = Gc = 1,\ Q = 0.3, M = 0.5, k = 0.1$ and $N = 1$. Moreover, the case of air ($Pr = Sc = 0.7$) is indicated by dotted lines and the methanol case at 25℃ ($Pr = 6.83$ and $Sc = 1.14$) is shown by solid lines, except the values that vary are mentioned explicitly in appropriate tables and figures.

TABLE 1 Comparison of $-f''(0)$ for various values A and for Newtonian fluid

A	Mukhopadhyay et al. [6]	Mahdy [7]	**Present Study**
0.8	1.261479	1.261012	1.261094
1.2	1.377850	1.377842	1.377929

TABLE 2 Comparison of present values of $-\theta'(0)$ for variation in Pr and M

M	Pr	Magyari and Keller [2]	El-Aziz [3]	Bidin and Nazar [4]	Ishak [5]	**Present Study**
0.0	1.0	0.954782	0.954785	0.9548	0.95478	0.954811
	2.0			1.4714	1.47146	1.471454
	3.0	1.869075	1.869072		1.86907	1.869069
	5.0	2.500135	2.500132		2.50012	2.500125
	10.0	3.660379	3.660372		3.66027	3.660379

Figs. (2a) – (2c) explicates the noticeable effect of M on $f'(\eta)$, $\theta(\eta)$ and $\phi(\eta)$ respectively. For both air and methanol, as the value of M increases, the fluid flow is resisted as a result of strong Lorentz force, which also leads to a drop in $f'(\eta)$. A subsequent increase in $\theta(\eta)$ and $\phi(\eta)$ are observed.

In figs. (3a) – (3c), the velocity profile, temperature distribution and concentration distribution are drawn versus η respectively for several values of A. The graph makes it crystal clear that enhancing A results in depreciation of $f'(\eta)$, $\theta(\eta)$ and $\phi(\eta)$. The reason behind this is that, A has a diminishing influence on the momentum boundary layer thickness. Moreover, the sheet transmits less solute and less heat to the fluid.

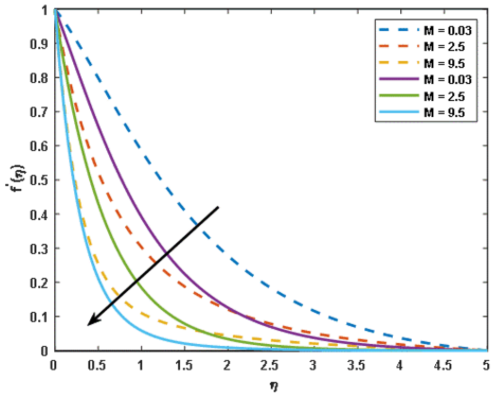

Fig. 2a Velocity profile for various *M*

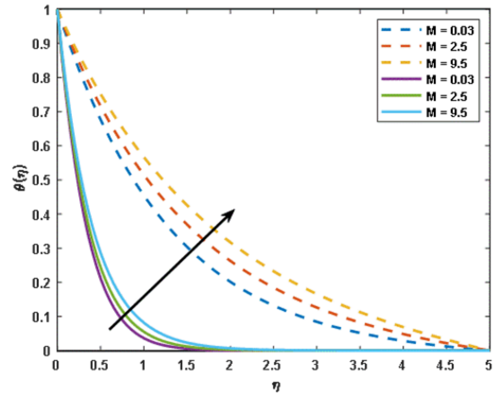

Fig. 2b Temperature distribution for various *M*

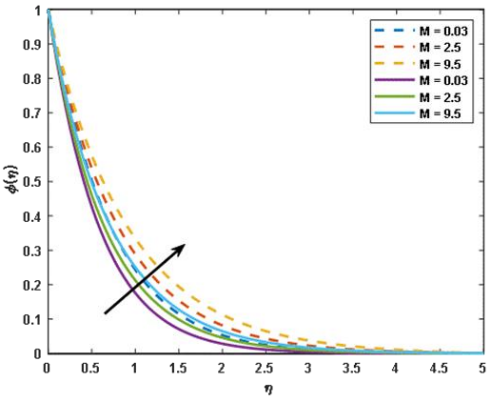

Fig. 2c Concentration distribution for various *M*

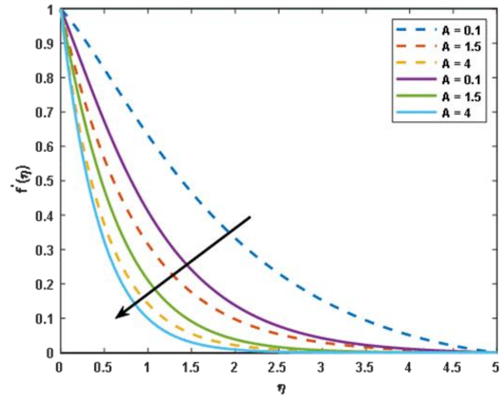

Fig. 3a Velocity profile for various *A*

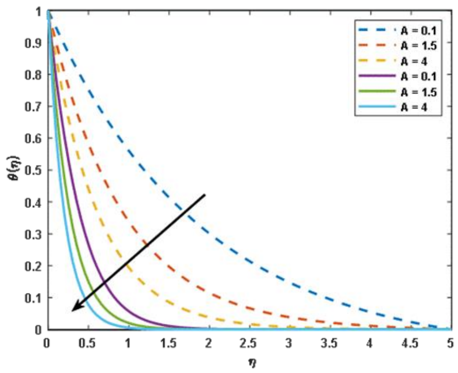

Fig. 3b Temperature distribution for various *A*

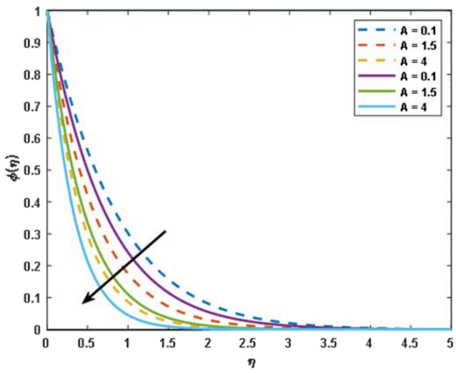

Fig. 3c Concentration distribution for various *A*

Figs. (4a) and (4b) are plotted to expose the impact of Gr on $f'(\eta)$ and $\theta(\eta)$. An inflation in the values of Gr, skyrockets the velocity $f'(\eta)$ which in-turn depreciates the temperature $\theta(\eta)$.

Similarly increasing the values of Gc, enhances the velocity $f'(\eta)$ and decreases the concentration distribution $\phi(\eta)$. This is seen vividly through figs. (5a) and (5b).

The effect of radiation parameter R are shown in figs. (6a) and (6b). It has been perceived that increasing the values of R has the tendency to rise both $f'(\eta)$ and also $\theta(\eta)$ in the boundary layer.

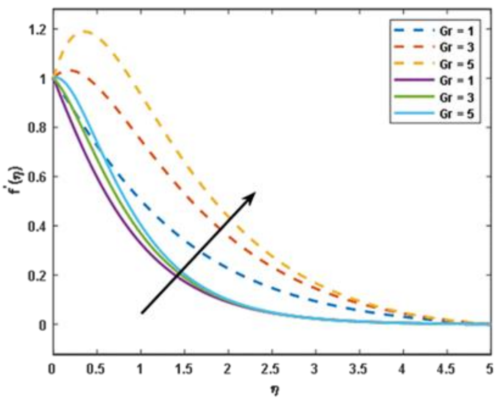

Fig. 4a Velocity profile for various Gr

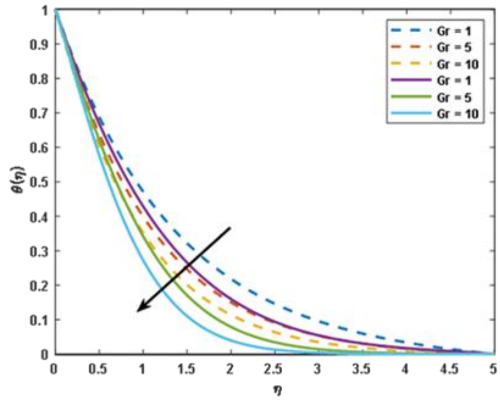

Fig. 4b Temperature distribution for various Gr

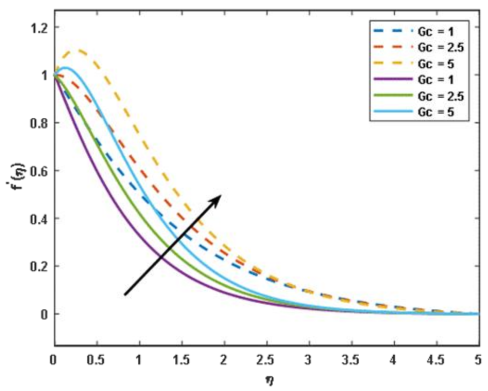

Fig. 5a Velocity profile for various Gc

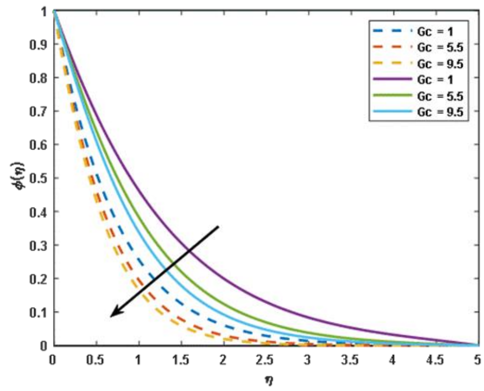

Fig. 5b Concentration distribution for various Gc

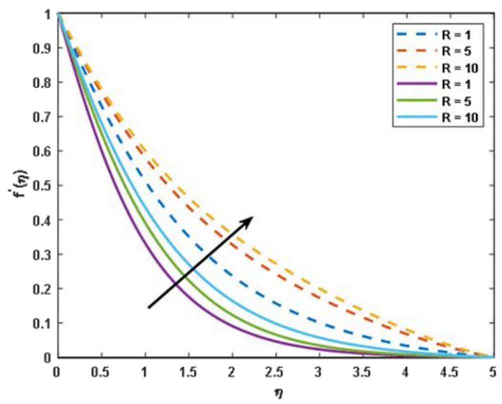

Fig. 6a Velocity profile for various R

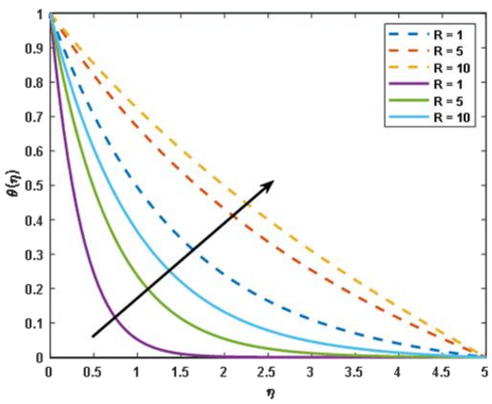

Fig. 6b Temperature distribution for various R

Fig. (7) illustrates how the fluid temperature behaves when the values of Q gets altered. Enhancing the values of Q led to a significant rise in $\theta(\eta)$. Similarly, fig. (8) shows that a rise in the values of Ec causes an escalation in the temperature distribution $\theta(\eta)$.

The concentration distribution $\phi(\eta)$ for disparate k values is plotted in fig. (9). Owing to the fact that species conversion results via chemical reactions, augmenting the values of k brings down the boundary layer concentration.

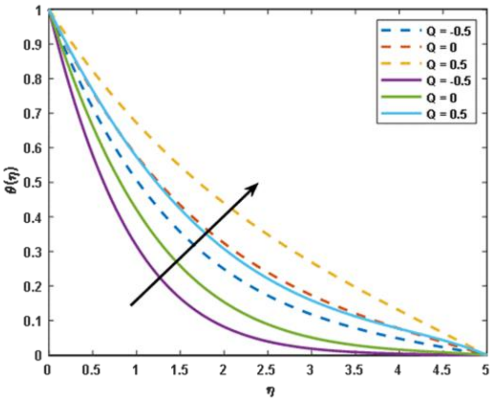

Fig. 7 Temperature distribution for various Q

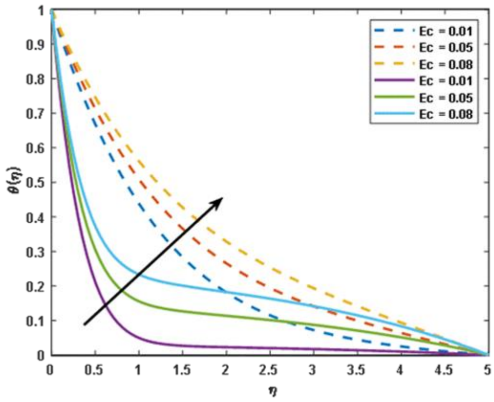

Fig. 8 Temperature distribution for various Ec

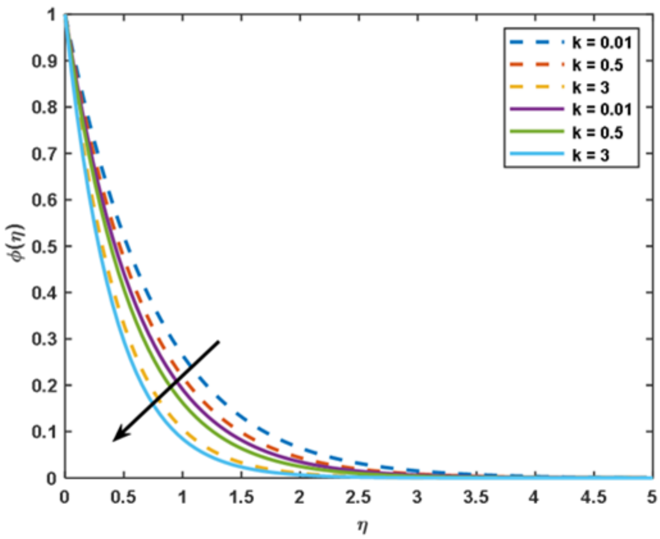

Fig. 9 Concentration distribution for various k

Figs. (10a) – (10c) depicts the striking instigation of N on velocity profile, temperature and concentration distributions respectively. $f'(\eta)$, $\theta(\eta)$ and $\phi(\eta)$ decreases as N increases. This depreciation is attributable to the heat being transmitted from the wall to the fluid nearby, which consequently pushes the particles to migrate away from the wall.

Augmenting the values of β has a decreasing impact on the velocity profile. On the contrary, the fluid's temperature was noticed a minute boost as β increases. These are explicitly observed through figs. (11a) and (11b).

Fig. (12) exemplifies how the boundary layer thickness suppresses as Pr intensifies. Notable changes for different values of Pr under different values of exponential parameter N was witnessed.

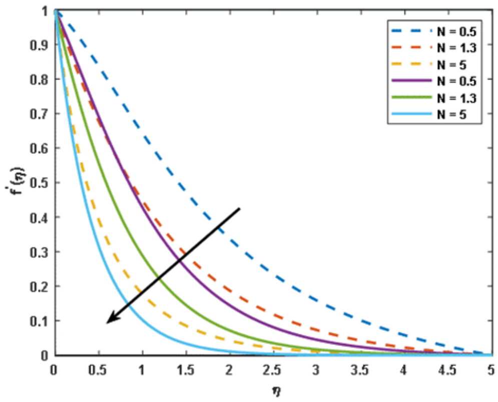

Fig. 10a Velocity profile for various N

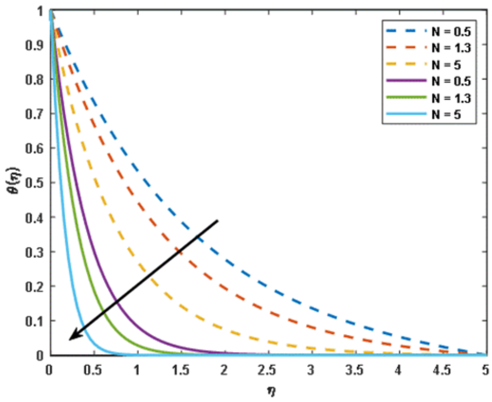

Fig. 10b Temperature distribution for various N

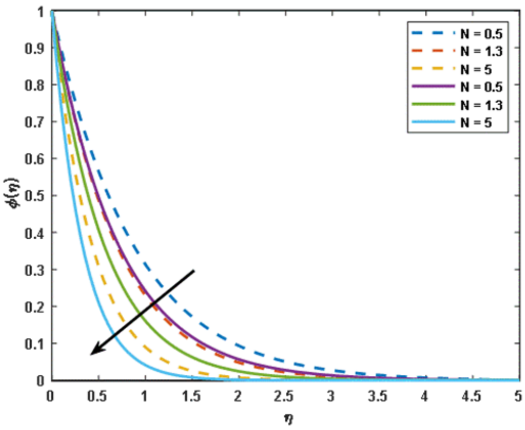

Fig. 10c Concentration distribution for various N

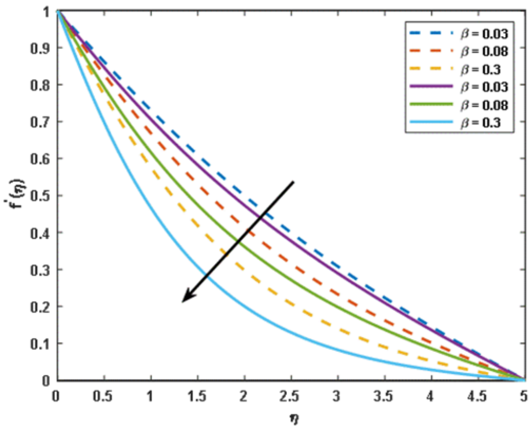

Fig. 11a Velocity profile for various β

The concentration distribution's behaviour for a range of Sc values in the case of air and methanol can be found in fig. (13). The thickness of the solute boundary layer gets dwindled with escalation in the values of Sc. As a result, the concentration distribution $\phi(\eta)$ gets suppressed.

Figs. (14a) – (14c) illustrates the $f'(\eta)$, $\theta(\eta)$ and $\phi(\eta)$ versus η respectively for proliferating values of s. s has a depreciating influence on both the wall shear stress and $f'(\eta)$ in the boundary layer. Similarly, $\theta(\eta)$ and $\phi(\eta)$ are found to decrease with increasing s.

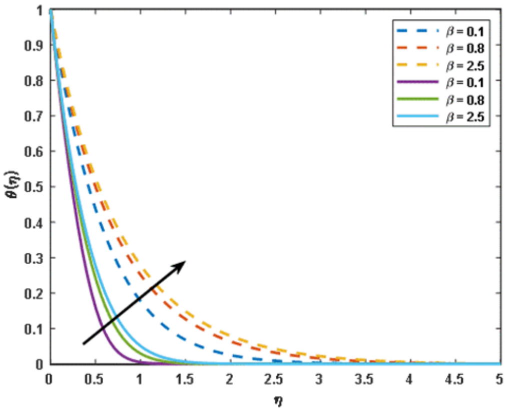

Fig. 11b Temperature distribution for various β

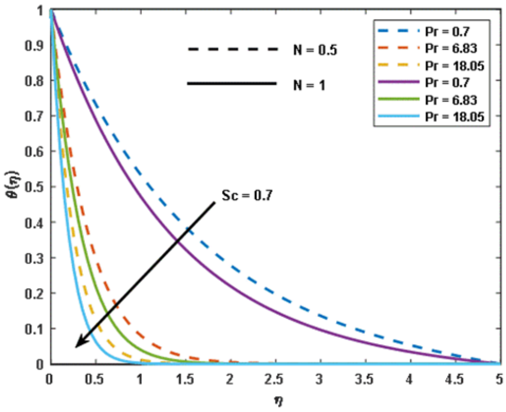

Fig. 12 Temperature distribution for various Pr

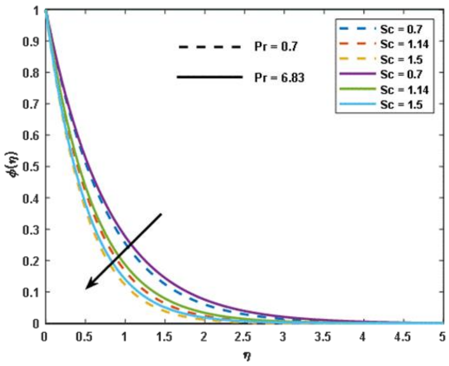

Fig. 13 Concentration distribution for various Sc

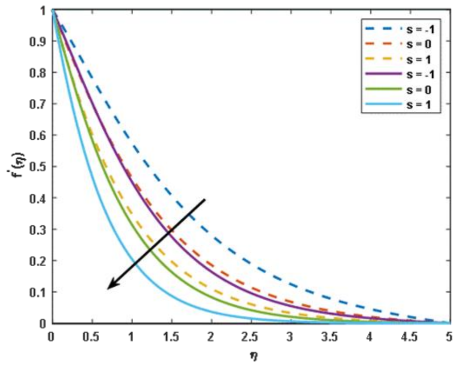

Fig. 14a Velocity profile for various s

The following results were concluded from the tabulated values of factors affecting C_f, Nu_x and Sh_x (Table 3). A rise in the value of M depreciates C_f, Nu_x and Sh_xwhereas the reverse trend is observed for thermal and solutal Grashof number. The value of friction factor gets declined, the Sherwood number and Nusselt number gets enhanced when the values of A, N and s gets proliferated. The reverse phenomena are observed for β. Enhancing R, Ec and Q increases C_f and Sh_x which consequently depletes Nu_x but the opposite discussion holds for Pr. The values of C_f and Nu_x gets suppressed but Sh_x gets intensified as the values of Sc and k increases.

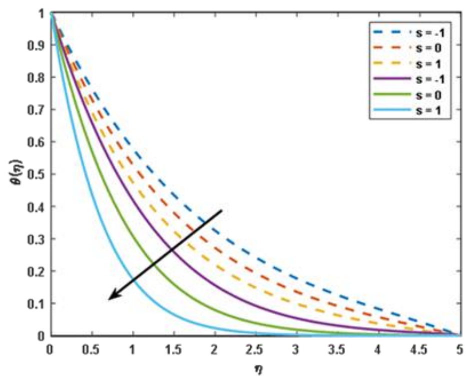

Fig. 14b Temperature distribution for various s

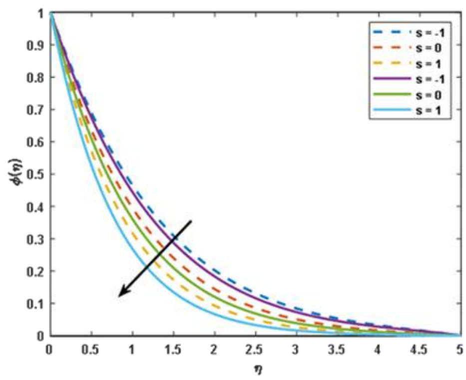

Fig. 14c Concentration distribution for various s

TABLE 3 The values of factors affecting C_f, Nu_x and Sh_x for several pertinent parameters

A	β	M	Gr	Gc	R	Ec	Q	k	N	s	Pr	Sc	$\left(1+\frac{1}{\beta}\right) f''(0)$	$-\theta'(0)$	$-\phi'(0)$
0.5	2	0.5	1	1	0.8	0.01	0.3	0.1	1	0.1	0.7	0.7	-0.9874	0.9528	1.55372
1													-1.4749	1.24926	1.93227
	2.5												-0.9339	0.95204	1.5529
		1											-1.3545	0.93734	1.53899
			2										-0.2824	0.97701	1.58042
				2									-0.4153	0.96831	1.57208
					1.5								-0.9325	0.78423	1.55767
						0.1							-0.9802	0.92353	1.55419
							0.5						-0.9705	0.8979	1.55492
								1					-1.0336	0.95013	1.82811
									5				-3.2543	1.5034	2.46016
										0.5			-1.1694	1.01992	1.70192
											6.83		-1.3632	3.37195	1.53131
												1.14	-1.0611	0.94856	1.98648

Conclusions

The following are the key findings observed in light of this study:

- Fluid velocity, temperature and concentration decreases significantly due to the rise in the A, N and s.
- Furthermore, increasing N enhances the heat and mass transfer rates.
- It's intriguing to comprehend that the influence of chemical reaction is so influencing, which ultimately augments the Sherwood number.
- The role of Q in $\theta(\eta)$ is vital for their effects on heat transfer are significant.
- In the absence of N, Q and for Newtonian fluid, the outcomes match those of Ishak [5].

Funding

No funding was received to assist with the preparation of this manuscript.

Conflict of Interest

The authors have no conflicts of interest to declare.

References

[1] L. J. Crane, "Flow past a Stretching Plate," Zeitschrift für Angewandte Mathematik und Physik (ZAMP), Vol. 21, No. 4, pp. 645–647, 1970.
[2] E. Magyari and B. Keller, "Heat and mass transfer in the boundary layers on an exponentially stretching continuous surface," Journal of Physics D: Applied Physics, Vol. 32, No. 5, pp. 577–585, 1999.
[3] M. Abd El-Aziz, "Viscous dissipation effect on mixed convection flow of a micropolar fluid over an exponentially stretching sheet," Canadian Journal of Physics, Vol. 87, No. 4, pp. 359–368, 2009.
[4] B. Bidin and R. Nazar, "Numerical solution of the boundary layer flow over an exponentially stretching sheet with thermal radiation," European Journal of Scientific Research, Vol. 33, No. 4, pp. 710–717, 2009.
[5] A. Ishak, "MHD Boundary Layer Flow Due to an Exponentially Stretching Sheet with Radiation Effect," Sains Malaysiana, Vol. 40, No. 4, pp. 391–395, 2011.
[6] S. Mukhopadhyay, P. De Ranjan, K. Bhattacharyya and G. C. Layek, "Casson Fluid Flow over an Unsteady Stretching Surface," Ain Shams Engineering Journal, Vol. 4, No. 4, pp. 933–938, 2013.
[7] A. Mahdy, "Unsteady MHD Slip Flow of a Non-Newtonian Casson Fluid due to Stretching Sheet with Suction or Blowing Effect," Vol. 9, No. 2, pp. 785–793, 2016.
[8] N. Casson, "A Flow Equation for Pigment-Oil Suspensions of the Printing Ink Type.," In: Mill, C.C., Ed., Rheology of Disperse Systems, Pergamon Press, Oxford, pp. 84–104, 1959.
[9] M. Q. Brewster, "Thermal Radiative Transfer and Properties," John Wiley& sons. Inc., New York, 1992.